Favourable scenarios established by SMBI for the realization of the ELMy H-mode at HL-2A*

Zheng-Ying Cui(崔正英)†, Yuan Xu(徐媛), Bei-Bin Feng(冯北滨), Yu-Hong Xu(许宇鸿), Xuan-Tong Ding(丁玄同), Xiao-Quan Ji(季小全), Yong-Gao Li(李永高), Zhong-Bing Shi(石中兵), Wu-Lv Zhong(钟武律), Min Jiang(蒋敏), Shao-Dong Song(宋绍栋), Jun Cheng(程均), Jin-Ming Gao(高金明), Jian-Yong Cao(曹建勇), Chun-Feng Dong(董春风), Kai Zhang(张凯), Cheng-Yuan Chen(陈程远), Mei Huang(黄梅), Qing-Wei Yang(杨青巍), Xu-Ru Duan(段旭如), and HL-2A Team

Southwestern Institute of Physics, Chengdu 610225, *China*

(Received 26 December 2016; revised manuscript received 7 April 2017; published online 20 June 2017)

The ELMy H-mode plasmas realized with the supersonic molecular beam injection (SMBI) are studied in relation to the energy confinement and the heating power for the L–H transition ($P_{\mathrm{L-H}}$) in the HL-2A tokamak. A database is assembled for this study based on the ELMy H-mode discharges during the experimental campaigns in the period 2009–2013 at the HL-2A tokamak. The statistical results show that the SMBI is favourable for reaching the H-mode by reducing the heating power at the L–H transition and for the H-mode performance by improving the energy confinement compared with the ordinary gas puffing (GP). The reduction of $P_{\mathrm{L-H}}$ is about 20% when the density is low, and the energy confinement enhancement factor of $H_{\mathrm{H98y2}} = \tau_{\mathrm{E}}/\tau_{\mathrm{th,98y2}} \approx 1.5$ is achieved with the SMBI. Note that in the database the density dependence of $P_{\mathrm{L-H}}$ is non-monotonic with the $\bar{n}_{\mathrm{e,min}} \approx 3\times10^{19}$ m^{-3} at which the $P_{\mathrm{L-H}}$ is minimum. Most of $P_{\mathrm{L-H}}$ data are on the low density branch where the $P_{\mathrm{L-H}}$ increases with the decrease in density. The minimum of the $P_{\mathrm{L-H}}$ in HL-2A is comparable to the ITPA multi-machine threshold power scaling $P_{\mathrm{thr_scal08}}$. The physics behind the reduction of the $P_{\mathrm{L-H}}$ with the SMBI is also investigated in relation to the change of the density gradient at the plasma edge, the gas fuelling efficiency, and the recycling.

Keywords: ELMy H-mode, SMBI, L–H transition, energy confinement, database

PACS: 52.55.Fa, 52.55.Dy, 52.25.Fi **DOI:** 10.1088/1674-1056/26/8/085205

1. Introduction

The high confinement mode (H-mode), as a projected baseline operational scenario for the International Tokamak Experimental Reactor (ITER), can be realized in present-day devices when the heating power is above a certain value. One of the issues in the H-mode studies is to find a favorite condition for the transition from a low confinement mode (L-mode) to an H-mode with the lowest heating power and to precisely predict the critical power in ITER.[1,2] Although progress is being made in understanding the physics underlying the L–H transition, the mechanism of the L–H transition is still not fully understood. Many factors, such as the neutral density,[3,4] magnetic configuration,[5–11] toroidal rotation,[12] and radial electric field[13] can affect the transition. Zonal flows have also been reported to play an important role in the L–H transition.[14–16] Meanwhile, the influence of MHD activities on the L–H transition has also been discussed recently.[17] Therefore, the power needed for the L–H transition depends on many parameters. It is found that in many devices there are favourable plasma conditions by which the required power for the transition is relatively lowered. Under these conditions (deuterium plasma, the ion ∇B drift directed towards the working X-point) a power threshold scaling law has been deduced by analysing the ITER-like power threshold database,[2]

$$P_{\mathrm{thr-scal08}}(D) = 0.0488 B_{\mathrm{T}}^{0.803} \bar{n}_{\mathrm{e}}^{0.717} S^{0.941}, \quad (1)$$

where B_{T} is the toroidal magnetic field (in unit T), $\bar{n}_{\mathrm{e}}$ is the line-averaged electron density in the L-mode (10^{20} m^{-3}), and S is the plasma surface area (in unit m^2). Based on this scaling the minimum power to access the H mode in ITER is about 52 MW at $\bar{n}_{\mathrm{e}} = 0.5\times10^{20}$ m^{-3} and 86 MW at $\bar{n}_{\mathrm{e}} = 1.0\times10^{20}$ m^{-3}. The 95% confidence intervals are about 30 MW–100 MW for the low $\bar{n}_{\mathrm{e}}$ case and 50 MW–170 MW for the high $\bar{n}_{\mathrm{e}}$ case. Since the additional heating power available in the initial phase of ITER is limited, to precisely estimate and to lower the threshold power are of great importance.

In many devices, it has been found that the wall condition, fuelling and recycling play critical roles in the L–H transition. In ASDEX, the low recycling and refueling from the divertor chamber were favourable for the L–H transition.[18] In NSTX, the wall conditioning with lithium can reduce the threshold power and improve the H-mode performance.[19] Recently in EAST, a long-pulse H-mode was achieved after 5-kg lithium had evaporated into the vacuum vessel.[20] The lithium coat-

*Project supported by the National Natural Science Foundation of China (Grant Nos. 11375057 and 11175061) and the National Magnetic Confinement Fusion Science Program, China (Grant Nos. 2010GB102003 and 2014GB108003).

†Corresponding author. E-mail: cuizy@swip.ac.cn

© 2017 Chinese Physical Society and IOP Publishing Ltd

ing is considered as a key factor to reach this goal. In HL-2A, it was also found that the SMBI as a fuelling method is favourable for the L–H transition in comparison with the ordinary gas puffing. When the SMBI is applied, the edge particle recycling can be significantly reduced and the fuelling efficiency is increased by about 30%–60%.[21,22] The deep penetration of the molecular beam has been considered as a mechanism for the increase of the fuelling efficiency with the SMBI.[23]

On the other hand, it has been observed that the threshold power depends non-monotonically on the plasma density and exhibits a minimum value at a density denoted as $\bar{n}_{\mathrm{e,min}}$, in many devices. In ASDEX Upgrade, $\bar{n}_{\mathrm{e,min}} \approx 4\times10^{19}$ m^{-3}.[24] When the density is lower than $\bar{n}_{\mathrm{e,min}}$, the threshold power increases with density decreasing. This is known as the 'low-density branch'. The $\bar{n}_{\mathrm{e,min}}$ varies with plasma current I_{p} and B_{t} following a scaling $\bar{n}_{\mathrm{e,min}} = 0.7 I_{\mathrm{p}}^{0.34} B_{\mathrm{t}}^{0.62} a^{-0.95} (R/a)^{0.4}$ in 10^{19} m^{-3} using units in MA, T, and m.[25] It has been found that the ion heat flux played a significant role in the non-monotonic density dependence of the threshold power. The density at the minimum threshold power varies in different machines.[26–31] In the ITER-like power threshold database the $\bar{n}_{\mathrm{e,min}}$ decreases with plasma size and increases with magnetic field.[2] The power threshold at the low density branch is not well documented in these devices and at present no firm prediction is made for ITER. Therefore, it would be worth studying the H-mode property with relation to the L–H transition and the energy confinement in the HL-2A tokamak, especially the H-mode in the "low density branch" scenarios with the SMBI.

In the HL-2A tokamak, the H-mode with type-III edge localized modes (ELMs,) was first realized in 2009 by using the neutral beam injection (NBI) in combination with the electron cyclotron resonant heating (ECRH). With various wall-cleaning techniques, including siliconization, lithumization, and their combination to minimize the radiation power loss from impurities the ELMy H-mode discharges have been routinely obtained hereafter. So far, the minimum heating power to obtain the H-mode is about 0.52 MW with the NBI heating only. The H-mode in HL-2A has been mostly achieved with a marginal heating power at the low-density branch, where the heating power for the L–H transition ($P_{\mathrm{L-H}}$) decreases with increasing density. The $P_{\mathrm{L-H}}$ with the SMBI fueling is then studied statistically. The characteristics of the global energy confinement time are also investigated based on an assembly of the energy confinement database.

The rest of the present paper is organized as follows. The experiment condition and the related diagnostics are introduced in Section 2. The characteristics of the L–H transition power with the SMBI are presented in Section 3. Confinement properties of the H-mode are shown in Section 4. Finally, the results are summarized in Section 5.

2. Experimental conditions

The HL-2A device is a double-null divertor tokamak with a major radius R of 1.65 m and a minor radius a of 0.40 m. The typical parameters of the H-mode discharges presented in this paper are $B_{\mathrm{t}} = 1.27$ T–1.5 T and $I_{\mathrm{p}} = 150$ kA–180 kA. The plasma facing components in the HL-2A tokamak consist of carbon in the main chamber, carbon-fiber composite (CFC) on the baffle, and graphite tiles on the limiter, dome and armor plate for the neutral beam injection as illustrated in Fig. 1(a). Four pairs of fixed limiters and a segment of moveable limiter have often been used in the HL-2A discharges. A fraction of 30% of the vessel inner surface is covered by the graphite or the CFC. A detailed schematic view with these components is shown in Fig. 1(b). The lower-single-null (LSN) divertor configuration is implemented from the beginning of the discharge in order to reduce the plasma–wall interaction for the H-mode performance in the HL-2A. The bypasses between the divertor chamber and the main chamber near the baffles are closed in order to reduce the heating power for the L–H transition as

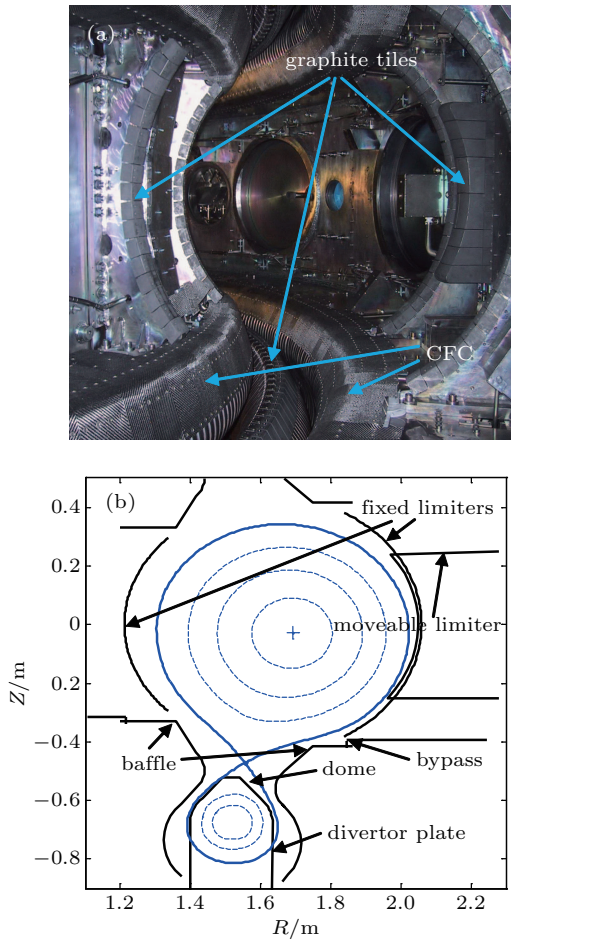


Fig. 1. (color online) (a) Tangential view of the central column of HL-2A with graphite tiles and (b) the poloidal cross section, showing the divertor configuration calculated by the EFIT code. The fixed and moveable limiters are covered by the graphite tiles, and the baffle and dome are covered by CFC.

suggested in Ref. [32]. The H-mode is realized in deuterium plasmas with the ion ∇B drift directed towards the lower X point, which is the working null in the single divertor operation configuration regime.

The NBI and ECRH are the primary auxiliary heating systems in the HL-2A tokamak. The maximum input power and the beam energy of the NBI are 1.2 MW and 45 keV, respectively. The working gas of the neutral beam source is deuterium for having optimal isotopic effects on the $P_{\mathrm{L-H}}$. The NBI heating power is tangentially co-injected with a maximum pulse duration of 0.8 s. The ECRH system consists of six gyrotrons (6×0.5 MW, 68 GHz) and launches in the second harmonic X-mode for the low toroidal magnetic field discharge. The ECRH scheme could provide 100% absorption in the electron channel with a narrow power deposition profile. A ray-tracing code C3PO/LUKE is applied to the absorbed ECRH power calculation.[33] A typical result for a discharge with plasma parameters of $I_{\mathrm{p}} = 184$ kA, $\bar{n}_{\mathrm{e}} = 1.2 \times 10^{19}$ m^{-3}, and $B_{\mathrm{t}} = 1.31$ T is presented in Fig. 2. The density and temperature profiles input into the code are also shown in Figs. 2(a) and 2(b). One can see that an ECRH power of 970 kW with 100% absorption is deposited at $\rho \sim 0.3$, where ρ is the normalized poloidal flux coordinate.

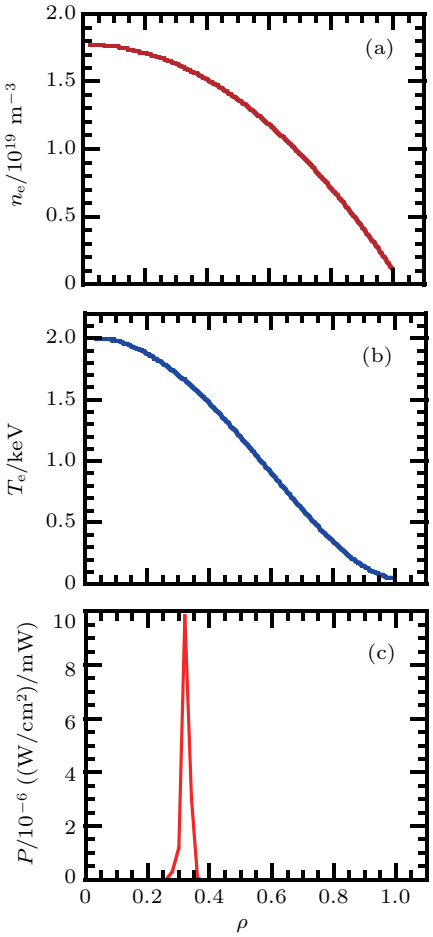


Fig. 2. (color online) (a) Electron density profile, (b) temperature profile used in the calculation, and (c) absorbed power of ECRH calculated with a ray tracing code C3PO/LUKE.

In the HL-2A tokamak the electron density profile is measured with an eight-chord 337-μm HCN laser interferometry[34] in the central part of the plasma ($\rho < 0.6$) and with a 26.5-GHz–50-GHz microwave (MW) reflectometer in the outer part of the plasma at which the density is less than 2.0×10^{19} m^{-3}.[35] The electron temperature profile is measured by the electron cyclotron emission (ECE) diagnostic, for which the spatial resolution and the time resolution are 2 cm and 10 μs, respectively.[36] The ECE signal amplitude is calibrated with the Thomson scattering diagnostic. The ion temperature profile is measured with an eleven-channel neutral particle analyzer and a ten-point charge exchange recombination spectrometer. The NBI heating power has been estimated by using an empirical scaling law, which includes some basic parameters, such as the averaged pressure in the discharge chamber of the ion sources, the averaged power loss ratio of the neutralization ducts and the averaged acceleration voltage of ion sources.[37] These parameters are all measured during plasma discharges. The input power of ECRH is measured with the calorimetric method.[38]

The SMBI has generally been used as one of the fuelling methods[39] in the HL-2A tokamak, where the ordinary gas puffing and pellet injection are also available for fuelling. Because of quick responses and the well-controlled particle quantity, the SMBI is also used for the density feedback control and other physics studies, such as the particle transport, ELM mitigation, and impurity transport, in the HL-2A tokamak.[40–42] The backing pressure and the pulse duration of the SMBI can be changed in ranges of 1 bar–30 bar (1 bar = 10^{-5} Pa) and 0.5 ms–5 ms, respectively. The injected deuterium molecular inventory is about 2×10^{17}–6×10^{19} and the velocity of the particles is about 1.3 km/s–1.8 km/s. Comparing with the ordinary gas puffing (GP), the increase of the fuelling efficiency for the SMBI is mainly due to the deep penetration and the edge cooling effect.[39,43] In general, the penetration depth of the neutral particles is about 4 cm–8 cm inside the last closed flux surface (LCFS) for the ohmic discharges. When the backing pressure of the SMBI increases, the penetration of the molecular particles becomes deeper.[44]

3. $P_{\mathrm{L-H}}$ with SMBI

In this paper, the heating power for the L–H transition is yielded as $P_{\mathrm{L-H}} = P_{\mathrm{ohm}} + P_{\mathrm{aux}} - \mathrm{d}W/\mathrm{d}t$, where P_{ohm} is the ohmic power, P_{aux} is the auxiliary heating power, and $\mathrm{d}W/\mathrm{d}t$ is the time variation of the total plasma energy. The radiation losses inside the separatrix are not subtracted in order to reduce the scatter of the data. The unusual high radiative discharges are excluded in the database and the ratio of the radiative power to the heating power is small ($< 20\%$). A comparison between the H-mode discharges achieved with the SMBI

(shot No. 11397, solid lines) and the GP (shot No. 11427, dashed lines) is plotted in Fig. 3. The time traces from the top to the bottom are (a) the plasma current and heating power of ECRH and NBI, (b) the line-averaged density, (c) the plasma stored energy, (d) the total radiated power in the main chamber, (e) the D_α emission in the main chamber, (f) the D_α in the divertor chamber, (g) the neutral particle pressure in the main chamber, $P_{\rm neu}$, (h) the neutral particle pressure in the divertor chamber, $P_{\rm neu-d}$, and (i) the control signals of the SMBI and GP fueling. They show that the plasma parameters are almost the same for the two discharges except for the auxiliary heating power and the neutral particle pressure in the main chamber. The input power of ECRH and NBI for the discharge with the SMBI (No. 11397) is about 1.5 MW ($P_{\rm ECRH} = 0.83$ MW and $P_{\rm NBI} = 0.67$ MW) while it is about 1.78 MW ($P_{\rm ECRH} = 1.12$ MW and $P_{\rm NBI} = 0.66$ MW) for the discharge with the GP (No. 11427). The $P_{\rm nue}$ in the discharge with the GP is nearly 3 times higher than that with the SMBI as shown in Fig. 3(g). Since the achieved electron density is similar for the two discharges (see Fig. 3(b)), the fuelling efficiency with the SMBI is therefore much higher than that with the GP. When the ECRH power is added to the NBI heated plasma, the L–H transitions happen to the two discharges with a sudden drop of the D_α signal displayed in Figs. 3(e) and 3(f). The line-averaged density $\bar{n}_{\rm e}$ and the plasma stored energy $W_{\rm dia}$ are then quickly increased. The L–H transition occurs at $t = 0.68$ s with $\bar{n}_{\rm e} = 1.73 \times 10^{19}$ m^{-3} in the discharge with the GP and at $t = 0.71$ s with $\bar{n}_{\rm e} = 1.62 \times 10^{19}$ m^{-3} in the discharge with the SMBI. The first ELM appears at $t = 0.7$ s in the GP H-mode and at $t = 0.73$ s in the SMBI H-mode. The energy confinement times measured by the diamagnetic loop are comparable to each other in the two H-mode discharges. This experiment indicates that with using the SMBI, which has the high fuelling efficiency and low neutral particle pressure, the L–H transition could happen under the lower heating power condition. A closer look in Fig. 3(b) further indicates that the electron density at the L–H transition in the discharge with the SMBI is lower than that with the GP. In HL-2A, the density dependence of the $P_{\rm L-H}$ mostly resides at the low density branch, which will be illustrated later in Fig. 8. The potential threshold power for the SMBI shot should be higher than that for the GP. Thus, the lower heating power for achieving the H-mode in the case of SMBI reveals that a favorable scenario is established by the SMBI fueling due to probably reduced edge recycling and ensuing influence on the edge profiles. Nevertheless, the heating power in the above two discharges might both exceed the L–H transition power threshold. Therefore, further investigation of the positive influence of the SMBI on the realization of the H-mode is necessary in the case of marginal heating power. Such a comparison between two discharges (with marginal heating power) is depicted in Fig. 4, where the L–H transition is realized with SMBI but not without the SMBI, under the same discharge conditions.

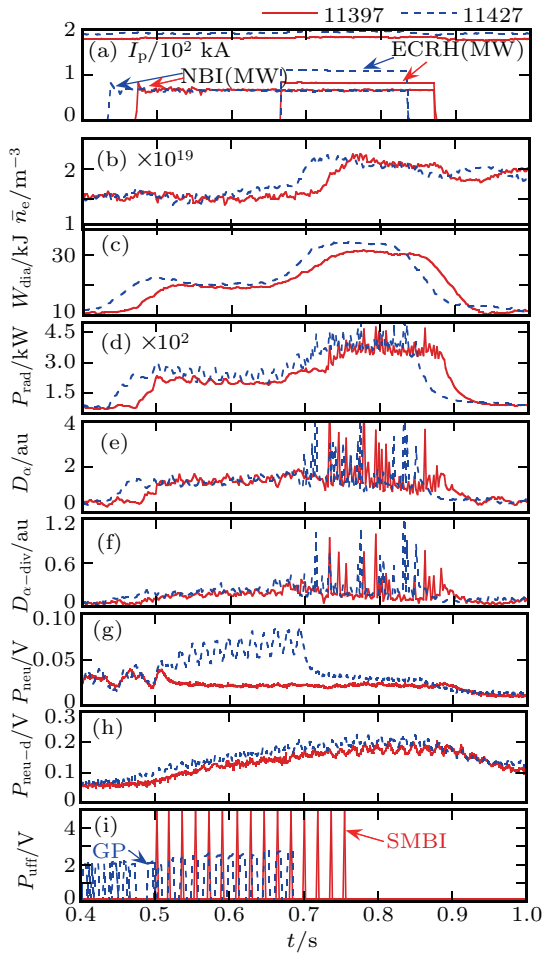


Fig. 3. (color online) Time traces of (a) plasma current and input power of ECRH and NBI, (b) line-averaged electron density, (c) plasma stored energy, (d) radiation power, (e) D_α in the main chamber, (f) D_α in the divertor chamber, (g) neutral particle pressure in the main chamber, and (h) neutral particle pressure in the divertor chamber, and (i) control signal of refueling for two discharges with SMBI and GP, respectively. The unit au is short for arbitrary unit.

The results are shown in Fig. 4 with two successive discharges. The main parameters of the plasmas are very similar. Both discharges have the same background gas puffing but not for the shot of No. 13723 where it has additional 4-pulse SMBI. Note the difference between Fig. 4 and Fig. 3, the amount of the SMBI in Fig. 4 is rather small so that the neutral particle pressures in both the main and divertor chambers are nearly unaffected after the molecular beam injection as shown in Figs. 4(g) and 4(h). The total input powers in the two discharges are also quite close, i.e., for shot No. 13722, $P_{\rm aux} = 1.58$ MW, ($P_{\rm ECRH} = 1.16$ MW and $P_{\rm NBI} = 0.42$ MW) and for No. 13723, $P_{\rm aux} = 1.56$ MW ($P_{\rm ECRH} = 1.15$ MW and $P_{\rm NBI} = 0.41$ MW). Before the first pulse of the SMBI at $t = 0.4$ s in shot No. 13723, the line-averaged densities are almost the same for the two discharges. When the ECRH power

is launched into the plasma at $t = 0.41$ s the electron density is strongly reduced by half due to the so-called 'particle pump-out effect'.[45] In the discharge with the SMBI a small increase of the density is observed following each SMBI pulse. At the time $t = 0.56$ s (marked by the vertical line) the L–H transition takes place at $\bar{n}_e = 1.1 \times 10^{19}$ m^{-3} when the fourth pulse of the SMBI is injected. After that, the $\bar{n}_e$ increases substantially and meanwhile the D_α in the divertor chamber drops. The first ELM appears at $t \approx 0.58$ s. However, for the discharge without the SMBI, the L–H transition does not happen even if the line-averaged density is increased gradually with the NBI heating and reaches the same value at which the L–H transition has already happened in the SMBI discharge as indicated by the horizontal line in Fig. 4(b). These results clearly show that the SMBI plays a favorable role in inducing the L–H transition with the marginal heating power.

In order to affirm the above conclusion, a statistical study on the heating power for the L–H transition, P_{L-H}, in discharges with and without the SMBI is necessary. A database in relation to the heating power just before the L–H transition was assembled with all the data available during the experimental campaigns in the period 2009–2013. More than 270 observations are included in the database. The details of the database are listed in Table 1.

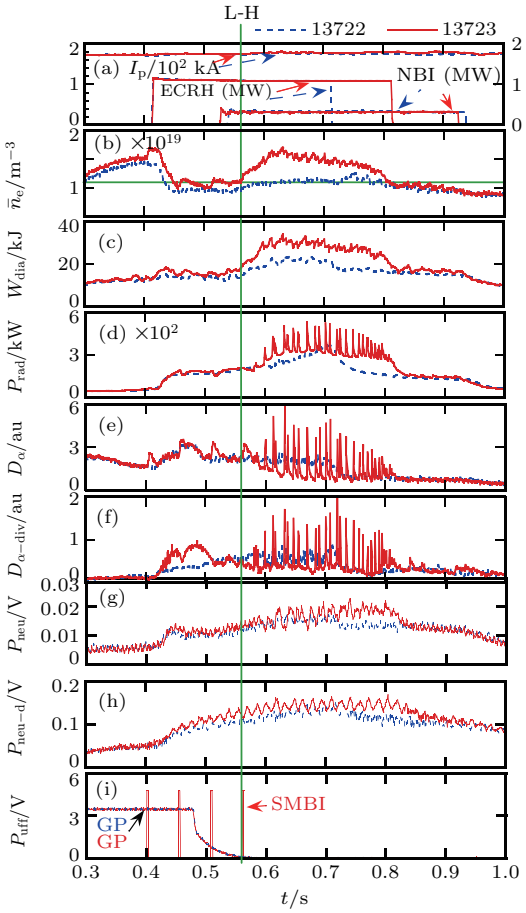


Fig. 4. (color online) Time evolutions of plasma parameters for two discharges with and without SMBI. The heating powers for the two discharges are the same. The H-mode can only be achieved with the SMBI.

Table 1. Range of main parameters for the H-mode power threshold database in the HL-2A tokamak.

No.	Dataset	Experimental campaign	Fueling method	Auxiliary heating	Observations	Range of main parameters
1	Threshold_SMBI_NBEC	2009–2013	SMBI	ECRH	160	127 kA $< I_p <$ 191 kA
						1.26 T $< B_t <$ 1.4 T
						1.08×10^{19} m^{-3} $< \bar{n}_e < 1.97 \times 10^{19}$ m^{-3}
				NBI		0.25 MW $< P_{ECRH} <$ 1.27 MW
						0.25 MW $< P_{NBI} <$ 1.13 MW
						0.64 MW $< P_{L-H} <$ 1.52 MW
2	Threshold_SMBI_NB	2009–2013	SMBI	NBI	44	156 kA $< I_p <$ 195 kA
						1.3 T $< B_t <$ 1.41 T
						1.46×10^{19} m^{-3} $< \bar{n}_e < 2.88 \times 10^{19}$ m^{-3}
						0.71 MW $< P_{NBI} <$ 1.15 MW
						0.52 MW $< P_{L-H} <$ 1.16 MW
3	Threshold_GP_NBEC	2009–2013	GP	ECRH	20	142 kA $< I_p <$ 181 kA
						1.28 T $< B_t <$ 1.38 T
						1.25×10^{19} m^{-3} $< \bar{n}_e < 2.13 \times 10^{19}$ m^{-3}
				NBI		0.35 MW $< P_{ECRH} <$ 1.75 MW
						0.46 MW $< P_{NBI} <$ 1.09 MW
						1.12 MW $< P_{L-H} <$ 2.11 MW
4	Threshold_ GP_NB	2009–2013	GP	NBI	46	141 kA $< I_p <$ 185 kA
						1.26 T $< B_t <$ 1.41 T
						1.43×10^{19} m^{-3} $< \bar{n}_e < 3.20 \times 10^{19}$ m^{-3}
						0.80 MW $< P_{NBI} <$ 1.10 MW
						0.52 MW $< P_{L-H} <$ 1.62 MW

Considering the effect of ECRH on the particle transport, the L–H transition with the combination of ECRH and NBI are separated from the transition with NBI only in the database. The comparison of the $P_{\mathrm{L-H}}$ between the SMBI and the GP (without SMBI) shots is shown in Fig. 5, where the H-mode discharges achieved with the ECRH and NBI are plotted in Fig. 5(a) and those with NBI only are presented in Fig. 5(b). The relatively low density range in Fig. 5(a) is attributed to the ECRH "pump-out" effect on plasma particles. From Figs. 5(a) and 5(b) it follows that the $P_{\mathrm{L-H}}$ with the SMBI is obviously lower than that with the GP. In the cases of ECRH and NBI heating, the reduction of the $P_{\mathrm{L-H}}$ with the SMBI is more pronounced than that in the case of using NBI only. In the former case the averaged reduction of $P_{\mathrm{L-H}}$ reduces about 20% while in the latter one the reduction of $P_{\mathrm{L-H}}$ is just about 10%. In general, the SMBI pulse can cause a small increase of the density as shown in Fig. 4. Thus, the reduction of the heating power for the L–H transition with using the SMBI could be due to the increase of the electron density at the low density branch. However, as illustrated in Fig. 4, the L–H transition is not realized in the GP discharge (without SMBI) at the same density as that for the L–H transition to appear in the SMBI shot. Therefore, the increase of the density cannot be the only reason for the significant reduction of the $P_{\mathrm{L-H}}$. Other mechanisms, such as the change in edge density and temperature profiles induced by the SMBI, should also be surveyed as possible causes to reduce the $P_{\mathrm{L-H}}$ in the SMBI discharges.

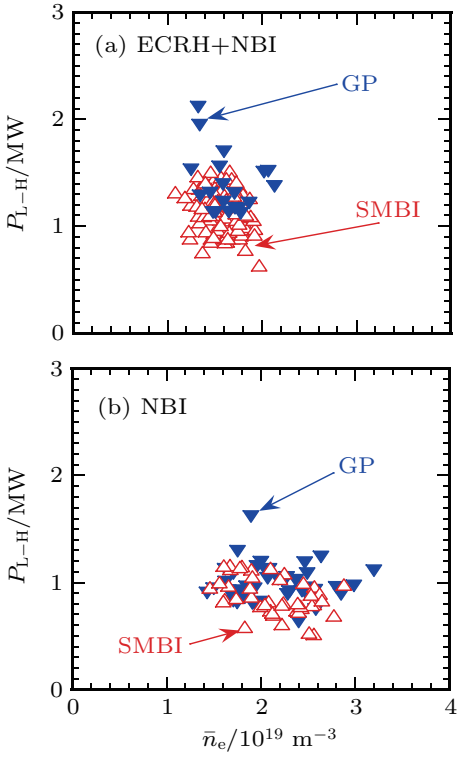


Fig. 5. (color online) Comparison of the heating power for the L–H transition between the GP and SMBI with (a) combination of ECRH and NBI and (b) NBI only.

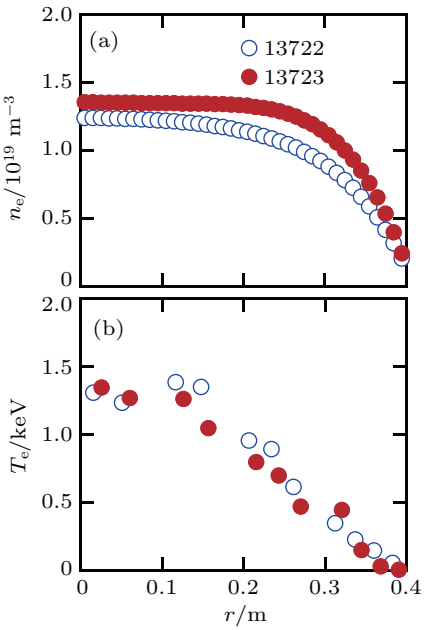


Fig. 6. (color online) Radial profiles of (a) electron density and (b) temperature for the discharges presented in Fig. 4.

Figure 6 shows the comparisons of the density and temperature profiles between the two discharges shown in Fig. 4. The data are taken at the time $t = 0.52$ s after the injection of the third SMBI pulse. It shows that the density increases significantly in the outer part of the plasma with the SMBI injection. The temperature profile measured with the ECE diagnostic, however, does not change too much. For these two discharges, the MW reflectometer is unfortunately not available to measure the edge plasma density. The density profiles in Fig. 6(a) are obtained by the Abel inversion method with the outermost channel of the HCN laser interferometry up to $r = 0.25$ m. Therefore, the density and temperature profiles from another discharge, where the MW reflectometer is usable, are compared in Fig. 7. The discharge conditions and the plasma parameters are similar to those in shot No. 13723. The profiles are taken just before and after the SMBI pulse prior to the L–H transition. In Fig. 7(a), the density denoted by diamonds in the core region is measured by the laser interferometry and the circles in the outer plasma was measured by the MW reflectometer. The temperature is measured by the ECE system. Considering the optical thickness of the plasma the temperature profile in a region of $\rho < 0.95$ is reliable in the highly heated plasmas. Figure 7(a) shows that the density increases considerably in a region of 0.2 m $< r(\mathrm{m}) <$ 0.35 m with the SMBI. The largest increment is about 10% at the location $r = 0.27$ m. On the other hand, the change in the temperature is trivial as shown in Fig. 7(b). Thus, the gradient of the pressure ($P = nT$) is enhanced significantly with the injection of the SMBI, especially at the edge region. The important change of $\mathrm{d}P/\mathrm{d}r$ can be seen in the outer part of the plasma as shown in Fig. 7(c). A deep pressure gradient well is formed at

$r = 0.28$ m by reducing 24% with the SMBI. Thus, the E_r may also be changed in the edge region. Since turbulence could be stabilized by a perpendicularly sheared $E_r \times B$ flow, a reduction of the power threshold can therefore be expected. This might be one of the reasons for the reduction of the heating power for the L–H transition with the SMBI.

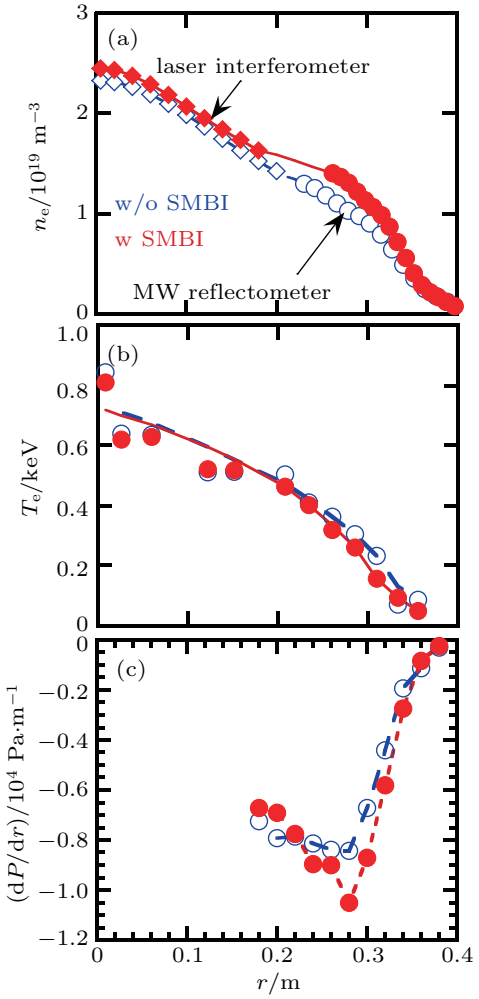


Fig. 7. (color online) Radial profiles of (a) electron density, (b) temperature, and (c) pressure gradient before and after the SMBI.

With the favorable SMBI, a lot of H-mode discharges are obtained with the marginal heating power in the HL-2A tokamak. All the data with the SMBI in the HL-2A H-mode power threshold database are presented in Fig. 8. It includes the ECRH and NBI heating. In the HL-2A tokamak, the H-mode plasmas with the high toroidal magnetic field ($B_t > 2.0$ T) are also realized. As shown in formula (1), the power threshold of the H-mode strongly depends on B_t. Presented in Fig. 8 are the data with the B_t in a range of 1.26 T–1.41 T. The study on the high B_t H-mode will be addressed in the future. In this database, the lowest density is about 1.1×10^{19} m^{-3} in the heating regimes of ECRH and NBI. The lowest P_{L-H} is about 0.52 MW under the condition of NBI heating only. An envelope curve (dash lines) for the lowest P_{L-H} against $\bar{n}_e$ is drawn for the HL-2A data. The data can be fitted by a formula $P_{L-H}^{fit} \sim n_e^{-0.7}$ and it shows a low density branch character. In this figure, the power threshold of P_{thr_scal08} is also shown by a solid line for a comparison. For the HL-2A data, the $\bar{n}_{e,min}$, at which the heating power is minimum, seems to be around $(2.6\sim3)\times10^{19}$ m^{-3} and is close to the P_{th_scal08}. The lack of high density data in the HL-2A database is mainly due to the limitation of the additional heating power. Moreover, the density is also limited by the ECRH cut off in the X-mode when the toroidal magnetic field B_t is low.

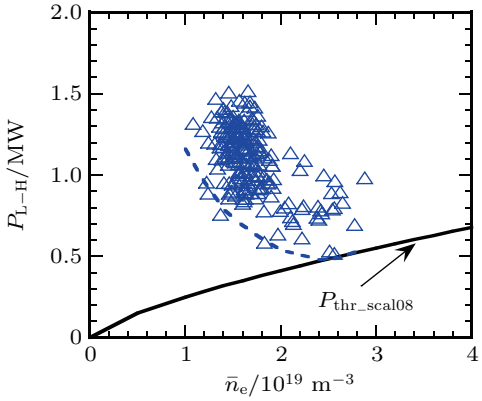


Fig. 8. (color online) P_{L-H} as a function of $\bar{n}_e$ for all the H-mode data with SMBI.

4. Confinement

Based on an assembly of the energy confinement database the characteristics of the energy confinement of the HL-2A H-mode with the SMBI are studied. The energy confinement time is defined as $\tau_E = W/(P_{tot} - dW/dt)$, and measured by the diamagnetic loops. Here, W is the plasma stored energy and P_{tot} is the total heating power. All the parameters at the time slice take an average over a time interval $\Delta t = \pm 20$ ms for the global energy confinement database. The energy confinement database of the HL-2A H-mode is collected when $\bar{n}_e$ or W_p reaches its maximum. The discharges with high radiation, $P_{rad}/P_{tot} > 0.6$, where $P_{tot} = P_{aux} + P_{ohm}$, is excluded.[2,46] The ranges of the plasma parameters in this database are as follows: 137 kA $< I_p <$ 196 kA, 1.26 T $< B_t <$ 1.41 T, 1.2×10^{19} m^{-3} $< \bar{n}_e < 3.9 \times 10^{19}$ m^{-3}. The energy confinement time is plotted as a function of $P_{loss} = P_{ohm} + P_{aux} - dW/dt$ in Fig. 9, where the H-modes with the GP are also presented for comparison. For making a succinct comparison, the H-mode data presented in Fig. 9 are those realized only with the NBI heating. As shown in the figure, the energy confinement time, τ_E, decreases with the increase of lost power. When the P_{loss} is low, the H-modes with higher τ_E are mostly obtained with the SMBI. This is also consistent with the previous result that the SMBI is favorable for the L–H transition with reduced heating power, particularly in the low heating power case. The IPB98(y, 2) scaling law with the $\sim P_{loss}^{-0.69}$ dependence is plotted in Fig. 9 by the dash lines, indicating that the characteristic of the HL-2A H-mode confinement is in agreement with the ITER scaling law IPB98(y, 2).

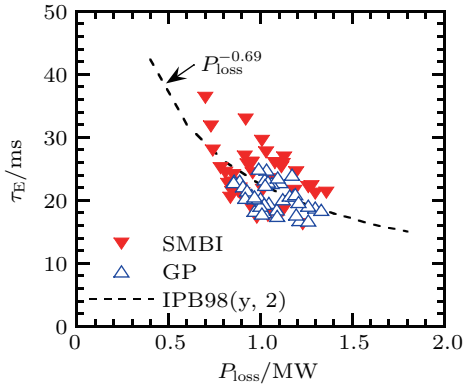


Fig. 9. (color online) Plot of energy confinement time versus heating power for the H-mode with SMBI and GP. The H-modes with NBI only are presented.

The comparison of the H-mode energy confinement time between the HL-2A data and the scaling law IPB98(y, 2) is shown in Fig. 10. The H-modes here are realized with various types of auxiliary heating regimes and fuelling methods. The result shows that the experimental energy confinement time for the HL-2A ELMy H-mode is in consistent with that from the IPB(98y, 2) by the confinement enhancement factor, $H_{\rm H98y2} = \tau_{\rm E}/\tau_{\rm th,98y2}$, ~ 1 in average. The $H_{\rm H98y2}$ factor for the H-modes with NBI only is generally higher than that with the combination of ECRH and NBI heating. This appears to be reasonable as the energy confinement is usually deteriorated with increasing heating power. It is also found that the energy confinement for the H-mode with the SMBI is better than that with the GP. In addition, the results also reveal that most of the H-mode discharges heated by ECRH and NBI are realized with the SMBI in the HL-2A tokamak. These facts all indicate that the SMBI can establish a favorable condition for the L–H transition. To date the H-mode with ECRH only has not yet been obtained in HL-2A. It is worth noting in Fig. 10 that the H-mode with good confinement by $H_{\rm H98y2} \sim 1.5$ can be achieved with the SMBI. This would be useful for ITER.

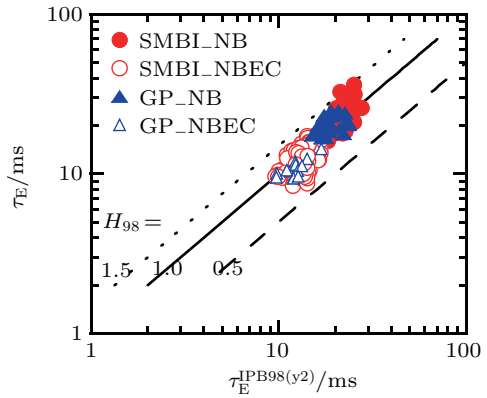


Fig. 10. (color online) Comparison of energy confinement time between the HL-2A experiment and the IPB98(y, 2) scaling law.

5. Summary

The heating power for the L–H transition and the energy confinement of the ELMy H-mode with the SMBI are statistically studied in the HL-2A tokamak. The experimental observation indicates that the SMBI is favorable for the L–H transition with reduced heating power when compared with the ordinary gas puffing. The reduction of the heating power with the SMBI to reach the H-mode is about 20% in the low density case. The fuelling efficiency and the electron pressure gradient at the edge are both significantly increased after the SMBI has been injected. Based on a database including 270 observations the characteristics of the transition power of the HL-2A H-mode with the SMBI are investigated. The experimental data reside mainly at the low density branch. The $\bar{n}_{\rm e,min}$, at which the heating power for the L–H transition is minimum, is in a range of $(2.6\sim3)\times10^{19}$ m^{-3}. When the density is lower than this value, the $P_{\rm L-H}$ increases with density decreasing.

The energy confinement of the H-mode with the SMBI is better than that with the GP based on the statistical study. The $H_{\rm H98y2}$ is around 0.6–1.5 for all the H-mode discharges obtained during the experimental campaigns in the period 2009–2013. A good confinement with $H_{\rm H98y2} \sim 1.5$ is achieved with the SMBI in the NBI heating plasmas.

Acknowledgement

The authors would like to thank Dr. Kardaun O J W F from IPP for his instruction and help in the creation of the HL-2A database, and also thank the HL-2A team for various diagnostics, data processing, and HL-2A operation.

References

[1] Ryter F and the H-mode Database Working Group 1996 *Nucl. Fusion* **36** 1217
[2] Martin Y R, Takizuka T and ITPA CDBM H-mode Threshold Database Working Group 2008 *J. Phys. Conf. Ser.* **123** 012033
[3] Maingi R, Kaye S M, Bell R E, Biewer T M, Chang C S, Gates D A, Gerhardt S P, Hosea J, LeBlanc B P, Meyer H, Mueller D, Park G Y, Raman R, Sabbagh S A, Stevenson T A and Wilson J R 2010 *Nucl. Fusion* **50** 064010
[4] Xu G S, Wan B N, Li J G, Gong X Z, Hu J S, Shan J F, Li H, Mansfield D K, Humphreys D A and Naulin V 2011 *Nucl. Fusion* **51** 072001
[5] Chang C S, Ku S and Weitzner H 2002 *Phys. Plasmas* **9** 3884
[6] Horton L D 2000 *Plasma Phys. Control. Fusion* **42** A37
[7] Andrew Y, Hawkes N C, O'Mullane M G, Sartori R, de Baar M, Coffey I, Guenther K, Jenkins I, Korotkov A, Lomas P, Matthews G F, Matilal A, Prentice R, Stamp M, Strachan J, de Vries P and JET EFDA Contributor 2004 *Plasma Phys. Control. Fusion* **46** A87
[8] McDonald D C, Cordey J G, Righi E, Ryter F, Saibene G, Sartori R, Alper B, Becoulet M, Brzozowski J, Coffey I, de Baar M, de Vries P, Erents K, Fundamenski W, Giroud C, Jenkins I, Loarte A, Lomas P J, Maddison G P, Mailloux J, Murari A, Ongena J, Rapp J, Pitts R A, Stamp M, Strachan J, Suttrop W and JET EFDA Contributor 2004 *Plasma Phys. Control. Fusion* **46** 519
[9] Gohil P, Jernigan T C, Scoville J T and Strait E J 2009 *Nucl. Fusion* **49** 115004
[10] Gohil P, Jernigan T C, Osborne T H, Scoville J T and Strait E J 2010 *Nucl. Fusion* **50** 064011
[11] Chang C S and Ku S 2008 *Phys. Plasmas* **15** 062510
[12] Politzer P A, Petty C C, Jayakumar R J, Luce T C, Wade M R, DeBoo J C, Ferron J R, Gohil P, Holcomb C T, Hyatt A W, Kinsey J, La Haye R J, Makowski M A and Petrie T W 2008 *Nucl. Fusion* **48** 075001
[13] Groebner R J, Burrell K H and Seraydarian R P 1990 *Phys. Rev. Lett.* **64** 3015

[14] Colchin R J, Schaffer M J, Carreras B A, McKee G R, Maingi R, Carlstrom T N, Rudakov D L, Greenfield C M, Rhodes T L, Doyle E J, Brooks N H and Austin M E 2002 *Phys. Rev. Lett.* **88** 255002

[15] Xu M, Tynan G R, Diamond P H, Manz P, Holland C, Fedorczak N, Chakraborty Thakur S, Yu J H, Zhao K J, Dong J Q, Cheng J, Hong W Y, Yan L W, Yang Q W, Song X M, Huang Y, Cai L Z, Zhong W L, Shi Z B, Ding X T, Duan X R, Liu Y and HL-2A Team 2012 *Phys. Rev. Lett.* **108** 245001

[16] Hidalgo C 2011 *Plasma Phys. Control. Fusion* **53** 074003

[17] Xu Y, Cheng J, Dong J Q, Dong Y B, Jiang M, Zhong W L, Yan L W, Shi Z B, Huang Z H, Li Y G, Nie L, Xu M, Zhao K J, Ji X Q, Yu D L, Liu Y, Cui Z Y, Chen W, Yang Q W, Ding X T, Duan X R, Liu Yong and the HL-2A Team 2015 *Plasma Phys. Control. Fusion* **57** 014028

[18] Wanger F, Becker G, Behringer K, Campbell D, Eberhagen A, Engelhardt W, Fussmann G, Gehre O, Gernhardt J, Gierke G V, Haas G, Huang M, Karger F, Keilhacker M, Klüber O, Kornherr M, Lackner K, Lisitano G, Lister G G, Mayer H M, Meisel D, Müller E R, Murmann H, Niedermeyer H, Poschenrieder W, Rapp H, Röhr H, Schneider F, Siller G, Speth E, Stäbler A, Steuer K H, Venus G, Vollmer O and Yü Z 1982 *Phys. Rev. Lett.* **49** 1408

[19] Maingi R, Bell R E, Canik J M, Gerhardt S P, Kaye S M, LeBlanc B P, Osborne T H, Bell M G, Fredrickson E D, Lee K C, Menard J E, Park J K, Sabbagh S A and NSTX Team 2010 *Phys. Rev. Lett.* **105** 135004

[20] Wan B N, Li J G, Guo H Y, Liang Y F, Xu G S, Wang L, Gong X Z and Garofalo A and Collaborators 2015 *Nucl. Fusion* **55** 104015

[21] Duan X R, Dong J Q, Yan L W, Ding X T, Yang Q W, Rao J, Liu D Q, Xuan W M, Chen L Y, Li X D, Lei G J, Cao J Y, Cao Z, Song X M, Huang Y, Liu Yi, Mao W C, Wang Q M, Cui Z Y, Ji X Q, Li B, Li G S, Li H J, Luo C W, Wang Y Q, Yao L H, Yao L Y, Zhang J H, Zhou J, Zhou Y and Liu Yong 2010 *Nucl. Fusion* **50** 095011

[22] Feng B B, Yao L H, Chen C Y, Ji X Q, Zhong W L, Shi Z B, Yu D L, Cui Z Y, Song X M and Duan X R 2013 *Acta Phys. Sin.* **62** 015203 (in Chinese)

[23] Rozhansky V, Senichenkov I, Veselova I, Morozov D and Schneider R 2006 *Nucl. Fusion* **46** 367

[24] Ryter F, Pütterich T, Reich M, Scarabosio A, Wolfrum E, Fischer R, Gemisic Adamov M, Hicks N, Kurzan B, Maggi C, Neu R, Rohde V, Tardini G and the ASDEX Upgrade Team 2009 *Nucl. Fusion* **49** 062003

[25] Ryter F, Rathgeber S K, Barrera Orte L, Bernert M, Conway G D, Fischer R, Happel T, Kurzan B, McDermott R M, Scarabosio A, Suttrop W, Viezzer E, Willensdorfer M, Wolfrum E and the ASDEX Upgrade Team 2013 *Nucl. Fusion* **53** 113003

[26] Snipes J, Granetz R S, Greenwald M, Kardaun O J W F, Kus A, Ryter F, Stroth U, Kollermeyer J, Fielding S J, Valovic M, DeBoo J C, Carlstrom T N, Schissel D P, Thomsen K, Campbell D J, Christiansen J P, Cordey J G, Righi E, Miura Y, Suzuki N, Mori M, Matsuda T, Tamai H, Fukuda T, Kamada Y, Matsuda T, Sato M, Takizuka T, Tsuchiya K and Kaye S M 1996 *Nucl. Fusion* **36** 1217

[27] Fielding S J, Ashall J D, Carolan P G, Colton A, Gates D, Hugill J, Morris A W, Valovic M, the COMPASS-D and ECRH Teams 1996 *Plasma Phys. Control. Fusion* **38** 1091

[28] Hubbard A E, Boivin R L, Drake J F, Greenwald M, In Y, Irby J H, Rogers B N and Snipes J A 1998 *Plasma Phys. Control. Fusion* **40** 689

[29] Carlstrom T N and Groebner R J 1996 *Phys. Plasmas* **3** 1867

[30] Fukuda T, Takizuka T, Tsuchiya K, Kamada Y, Nagashima K, Sato M, Takenaga H, Ishida S, Konoshima S, Higashijima S, Tobita K, Kikuchi M and Mori M 1997 *Nucl. Fusion* **37** 1199

[31] Andrew Y, Sartori R, Righi E, de la Luna E, Hacquin S, Howell D F, Hawkes N C, Horton L D, Huber A, Korotkov A, O'Mullane M G and JET-EFDA contributors 2006 *Plasma Phys. Control. Fusion* **48** 479

[32] Stroth U, Kaiser M, Ryter F and Wagner F 1995 *Nucl. Fusion* **35** 131

[33] Song S D, Liu Y, Zhang J H, He H D and Rao J 2007 *Nucl. Fusion Plasma Phys.* **27** 02-0123-04 (in Chinese)

[34] Zhou Y, Deng Z C, Liu Z T, Yi J, Tang Y W, Gao B Y, Tian C L, Li Y G and Ding X T 2007 *Rev. Sci. Instrum.* **78** 113503

[35] Zhong W L, Shi Z B, Zou X L, Ding X T, Huang X L, Dong Y B, Liu Z T, Xiao W W, Ji X Q, Cui Z Y, Liu Y, Yan L W, Yang Q W and Duan X R 2011 *Rev. Sci. Instrum.* **82** 103508 (in Chinese)

[36] Huang X L Shi Z B, Sun H J, Liu Z T, Cui Z Y and Ding X T 2011 *Nucl. Fusion Plasma Phys.* **31** 03

[37] Cao J Y, Wei H L, Liu H, Yang X F, Zou G Q, Yu L M, Li Q, Luo G W, Pan Y D, Jiang S F, Lei G J, Li B, Rao J and Duan X R 2015 *Chin. Phys. Lett.* **32** 052902

[38] Yao L H, Feng F. F, Chen C Y, Shi Z B, Yuan B S, Zhou Y, Duan X R, Sun H J, Lu J, Jiao Y M, Ni G Q, Lu H Y, Xiao W W, Li W, Pan Y D, Hong W Y, Ran H, Ding X T and Liu Y 2007 *Nucl. Fusion* **47** 1399

[39] Yao L H, Feng F. F, Chen C Y, Shi Z B, Yuan B S, Zhou Y, Duan X R, Sun H J, Lu J, Jiao Y M, Ni G Q, Lu H Y, Xiao W W, Li W, Pan Y D, Hong W Y, Ran H, Ding X T and Liu Y 2007 *Nucl. Fusion* **47** 1399

[40] Xiao W W, Zou X L, Ding X T, Yao L H, Feng B B, Song X M, Song S D, Zhou Y, Liu Z T, Yuan B S, Sun H J, Ji X Q, Gao Y D, Li Y G, Yan L W, Yang Q W, Liu Yi, Dong J Q, Duan X R, Liu Yong, Pan C H and HL-2A Team 2010 *Phys. Rev. Lett.* **104** 215001

[41] Chen C Y, Yao L H, Feng B B, Shi Z B, Zhong W L, Cheng J, Yu D L, Yang Q W and Duan X R 2012 24*th IAEA-FEC*, 8–13 October 2012, San Diego, USA, EX/6-3Rb

[42] Cui X W, Cui Z Y, Feng B B, Pan Y D, Zhou H Y, Sun P, Fu B Z, Lu P, Dong Y B, Gao J M, Song S D and Yang Q W 2013 *Chin. Phys. B* **22** 125201

[43] Cui Z Y, Zhou Y, Li W, Feng B B, Sun P, Dong C F, Liu Y, Hong W Y, Yang Q W and Ding X T 2009 *Chin. Phys. B* **18** 3473

[44] Zhou Y L, Wang Z H, Xu M, Wang Q, Nie L, Feng H, Sun W G 2016 *Chin Phys. B* **25** 095201

[45] Zou X L, Xiao W W, Song S D, Ding X T, Rao J, Zhou J, Huang M, Li L C, Yu D L, Yao L H, Feng B B, Chen C Y, Song X M, Zhou Y, Liu Z T, Sun H J, Shi Z B, Li Y G, Ji X Q, Liu Yi, Yan L W, Yang Q W, Dong J Q, Duan X R, Liu Yong and HL-2A Team 2010 23*rd IAEA FEC* (Daejeon, Korea, 2010) EXC/P8-20

[46] Ryter F and the H-mode threshold database group 2002 *Plasma Phys. Control. Fusion* **44** A415